Scientific Research Publishing

Open Journal of Fluid Dynamics, 2025, 15(1), 1-18
https://www.scirp.org/journal/ojfd
ISSN Online: 2165-3860
ISSN Print: 2165-3852

Study of Cylindrical Explosive Shock Waves at Air-Water Interface

Jayabal Rajasekar, Tae Ho Kim, Heuy Dong Kim*

Department of Mechanical Enigneering, Andong National University, Andong, South Korea
Email: *kimhd@anu.ac.kr

How to cite this paper: Rajasekar, J., Kim, T.H. and Kim, H.D. (2025) Study of Cylindrical Explosive Shock Waves at Air-Water Interface. *Open Journal of Fluid Dynamics*, **15**, 1-18.
https://doi.org/10.4236/ojfd.2025.151001

Received: December 10, 2024
Accepted: January 6, 2025
Published: January 9, 2025

Abstract

This study numerically analyzes the characteristics of shock wave propagation and attenuation in different mediums of explosion near the air-water interface (free surface). This study discussed flow physics like shock wave propagation, reflection, transmission, and cavitation qualitatively and quantitatively. The numerical simulation is carried out with air, water, and TNT (Tri Nitro Toluene), which were modeled using the ideal gas, Mie-Gruneisen (shock), and Jones-Wilkins-Lee (JWL) equation of state, respectively. The Coupled Eulerian-Lagrangian model is employed. In an explosion above the air-water interface, the shock wave propagates and reaches the free surface. Due to the acoustic impedance of water, the incident shock wave reflects, and part of the shock wave is transmitted into the water. The acoustic impedance of water is much higher than that of air, so this free surface acts like a solid wall. On the other hand, in an explosion below the interface, the incident shock wave reaches the free surface and the shock wave reflects as an expansion wave, resulting in cavitation. In an explosion at the free surface, shock wave propagates in both air and water; the propagation and attenuation of shock wave were studied. Hence, the free surface near the medium of explosion plays a significant role in the characteristics of shock propagation and attenuation effects.

Keywords

Explosion, Air-Water Interface, Cavitation, Unsteady Flow, Underwater, Acoustic Impedance

1. Introduction

Initially, researchers were interested in explosion-related studies due to military applications, but later, they extended their interest to various other fields. An explosion in any medium results in damage to structures and materials. However,

for the same amount of explosion, the characteristics of shock wave propagation vary for a different medium [1]. In explosion-related studies, the medium of explosion in which it is burst is critical. In an underwater explosion, the shock front interacts with either the free surface (water-air interface) or a fluid structure [2] [3]. In the free surface case, the incident and reflected shock cancel each other out near the interface, which results in cavitation [4]-[6]. In contrast, depending on the strength of the structure, the shock wave in fluid-structure interaction is either a compression wave or an expansion wave [7]-[9]. Numerous research studies have been published on explosions in water over the years. RH Cole published the similarity laws for calculating shock wave pressure in underwater explosions in 1948 [10]. Cavitation reloading near the free surface or structure is a very important parameter that is nearly equal to the incident shock and has a huge influence near the boundaries. The cavitation near the free surface, negative pressure profiles, and surface effects of underwater explosions were discussed by Kedrinskii *et al*. [11]. The effects of shock wave propagation and cavitation in underwater explosions near boundaries were discussed by Gaohui Wang *et al*. [12]. The phenomenon of air and underwater explosions and their influence on plane plates was reviewed by Rajendran and Lee [13]. The dynamic responses of fluid-structure interaction over the flat panel were studied by Librescu *et al*. [14]. Rajasekar *et al*. investigated the influence of numerical modeling of water through polynomial and the Mie-Gruneisen (shock) Equation of State in underwater explosions [15]. In recent years, underwater explosions have been subjected to computational analysis to determine the effects of a free surface, fluid-structure interaction, and cavitation. It also needs more attention to study the effect of the shock wave propagation and attenuation effects near the air-water interface.

In an air explosion, the shock wave propagates in the air and strikes either the structure or the free surface (air-water interface). Depending upon the acoustic impedance of the interacting object, the shock wave reflects and transmits as a compression/expansion wave [16]-[20]. In air explosions, most of the researchers were interested in unexpected accidents and their effects on civil structure, the impact of shock wave on the human body, especially traumatic brain injury, the effects on the environment due to explosions, mitigation of shock wave and small-scale experiments to study the effect of shock wave on different materials [21]-[26]. Liu *et al*. discussed different schemes involved in explosion and implosion in air [26]. While there are numerous studies related to air explosions, a comprehensive examination of the impact of a free surface near an air explosion on shock waves has not been undertaken thus far.

In an interface explosion, the shock wave transmits into both air and water at different magnitudes. The attenuation of the shock wave is different for air and water. Very few studies have been done on explosions at the interface [27]. Adrien *et al*. discussed the shape and dynamics of the cavity due to explosions at the water surface [28]. This interface explosion is a very interesting topic that many researchers have yet to explore. It has applications related to floating bombs in water

and many naval-related applications on the surface of the water. This study applies to military, civil, environmental, mining, naval, and medical fields. Shock waves occurring near the heterogeneous interfaces between liquid and gas exhibit highly complex behaviors, involving reflection, refraction, and occasionally cavitation phenomena. This field has attracted significant attention, not only for various engineering applications but also for its relevance to shock wave therapy and other medical applications. The use cases for this study vary depending on the magnitude of the shock wave and the medium of the explosion [29] [30]. Hence, explosion-related research was not reasonably well developed to study the characteristics of shock wave propagation and mitigation effects in different mediums of explosion near the free surface, and in-depth investigations are required. Hence, in this study, explosions below, above, and at the free surface were studied numerically. The main objective is to capture the shock wave propagation characteristics, attenuation, and cavitation effects near the air-water interface for different mediums of explosions.

During an explosion, the shock wave propagates from one medium to another either as a compression wave, or expansion wave. Depending on the medium of the explosion, the flow characteristics of the shock wave vary. Similarly, reflection and transmission phenomena also vary. This paper aims to investigate three different cases: 1) Underwater Explosion near free surface (the explosion in water); 2) The explosion above the free surface (explosion in air); and 3) Explosion at air-water interface (explosion at free surface). The shock wave propagation and attenuation characteristics in the different mediums near the free surface were carefully visualized, and the results were compared. For this study, a coupled numerical model is employed. This is a combination of the Eulerian and Lagrangian models. The Eulerian method is employed to model air with the ideal gas Equation of state (EOS), water with the Mie-Gruneisen (shock) Equation of State, and explosives with Jones, Wilkins, and Lee (JWL) equation of state. Hence, in this study, the shock wave reflection, transmission, cavitation, and attenuation effects near the free surface for different mediums of explosions are discussed qualitatively and quantitatively. This section is followed by: 2. Numerical Methods; 3. Validation; 4. Results; 5. Discussion; and 6. Conclusion.

2. Numerical Methods

2.1. Governing Equation

In this study, the Euler equations were solved using the Finite Volume Method (FVM) [31]. In this approach, the FVM solver solves flow field variables at each grid point for various time frames. The governing equations, such as the conservation of mass, momentum, and energy equations, were solved using the FVM approach. The equations are as follows:

$$\frac{\mathrm{d}}{\mathrm{d}t}\int_{v}\rho \mathrm{d}V+\int_{A}\rho\left(u\cdot n\right)\mathrm{d}A=0 \tag{1}$$

$$\frac{\mathrm{d}}{\mathrm{d}t}\int_{v}\rho u_i \mathrm{d}V + \int_{A}\rho u_i (u\cdot n)\mathrm{d}A = -\int_{A} pn_i \mathrm{d}A \tag{2}$$

$$\frac{\mathrm{d}}{\mathrm{d}t}\int_{v}\rho E \mathrm{d}V + \int_{A}\rho E (u\cdot n)\mathrm{d}A = -\int_{A} u\cdot pn\mathrm{d}A \tag{3}$$

where pressure, velocity, area, volume, density, and specific total energy are denoted as P, u, A, V, ρ, and E, respectively. The normal vector of each element face is represented by n. For an inviscid 2D compressible flow, we have

$$\frac{\partial U}{\partial t} + \frac{\partial F(U)}{\partial x} + \frac{\partial G(U)}{\partial y} = 0 \tag{4}$$

For gas flow, the equation is given as follows,

$$U = \begin{bmatrix} \rho \\ \rho u \\ \rho v \\ E \end{bmatrix}, F = \begin{bmatrix} \rho u \\ \rho u^2 + p \\ \rho uv \\ (E+p)u \end{bmatrix}, G = \begin{bmatrix} \rho v \\ \rho uv \\ \rho v^2 + p \\ (E+p)v \end{bmatrix} \tag{5}$$

where u and v are flow velocities in the x and y directions, respectively.

Explosives were modeled using Jones, Wilkins, and Lee (JWL) equation of state. The equation is as follows:

$$P = C_1\left(1-\frac{\omega}{R_1\upsilon}\right)\mathrm{e}^{-R_1\upsilon} + C_2\left(1-\frac{\omega}{R_2\upsilon}\right)\mathrm{e}^{-R_2\upsilon} + \frac{\omega E}{\upsilon} \tag{6}$$

where E and v are specific internal energy and specific volume, respectively. C_1, C_2, R_1, R_2, and ω are material constants. In this study, commercial hydrocode software is used, and values of all other constants are available in the hydrocode package [32]. Water and Air were modeled using Mie-Gruneisen (shock) and ideal gas equation of state and the equations are as follows:

$$P = P_r(\varepsilon_v) + \frac{\Gamma(v)}{v}\left[e - e_r\right] \tag{7}$$

$$P = (\gamma - 1)\frac{\rho}{\rho_0}E \tag{8}$$

where $\Gamma(v)$ is Gruneisen gamma, which is the thermodynamic property, and γ is the specific heat ratio ($\gamma = 1.4$).

2.2. Computational Domain

The computational domain is shown in **Figure 1**. The domain is 12 m in length and 10 m in height. The domain is symmetric about the Y axes. The lower half is filled with water and the upper half is filled with air, which is separated by an interface. Three cases were analyzed in this study. Case 1: Underwater Explosion near the free surface (explosion in water); Case 2: Explosion above the free surface (explosion in the air); and Case 3: Explosion at air-water interface (explosion at the free surface). TNT is used as a cylindrical explosive with a charge weight of 10 kg. The Euler sub-grid is employed to study the flow properties. The grid is equally

spaced, and the flow is allowed to pass through the material. The gauge points were fixed near the interface to monitor the pressure history. The numerical domain is modeled using a transmitting boundary condition. It reduces stress wave reflection from boundaries. The commercial software ANSYS workbench is used to model the simulations.

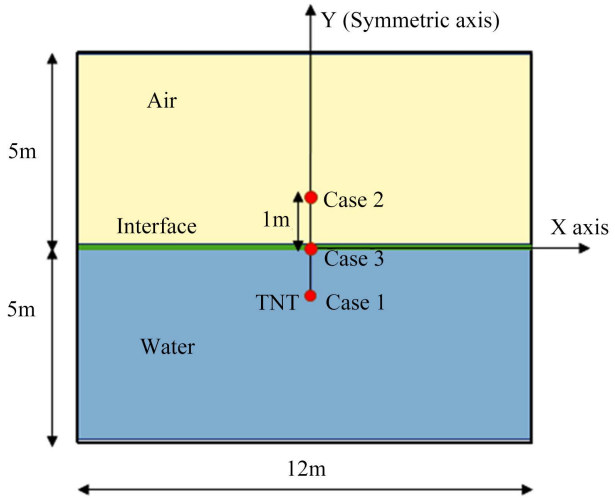

Figure 1. Computational domain for three cases. Case 1) Underwater explosion near the free surface, Case 2) Explosion above the free surface, and Case 3) Explosion at the air-water interface.

2.3. Grid Independence Study

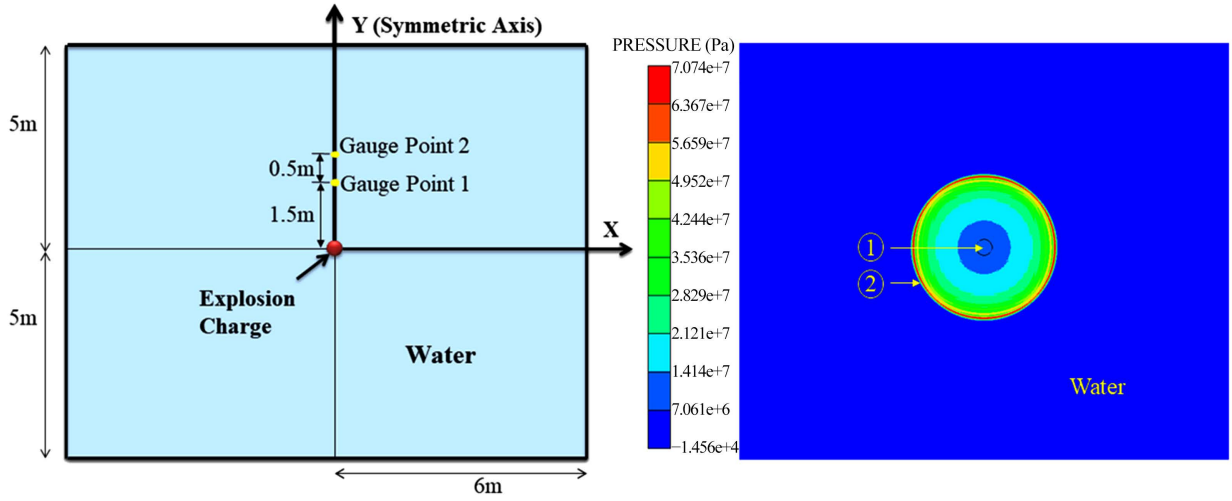

(a) (b)

Figure 2. (a) Computational domain of free field explosion; (b) Pressure contour of free field explosion at time t = 1 ms.

To validate the numerical model and perform a grid independence study, the computational domain of free field explosion is shown in **Figure 2(a)**. It is modeled with only water, and 10 kg of TNT is fixed at the center of the domain. The monitoring point was fixed at 1.5 and 2 m meters from the explosion. These do-

main dimensions and other boundary conditions remain the same as in Figure 1. The grid independence study has been carried out for underwater explosions using five different grids of 0.3, 0.53, 0.768, 1.2, and 2.13 million cells, and each mesh corresponds to a physical length ($\Delta x = \Delta y$) of 20 mm, 15 mm, 12.5 mm, 10 mm, and 7.5 mm, respectively. These simulations were carried out on five different grids, as mentioned above. The flow field variables were monitored at the gauge point fixed at 1.5 m and 2 m above the explosion. The peak pressures measured at 1.2 and 2.13 million grid cells predict similar results, and the difference is negligible, as shown in Figure 3. So, a further increase in mesh does not impact the results. Hence, considering the computational time, a physical length ($\Delta x = \Delta y$) of 10 mm and 1.2 million cells are used in this study.

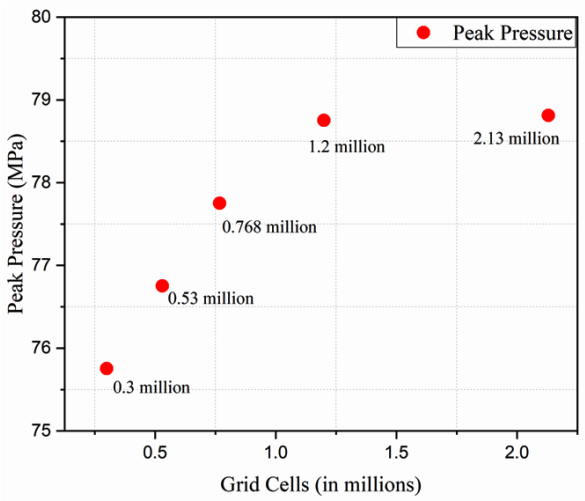

Figure 3. Peak pressure calculation for different grid sizes at 1.5 m from the center of the explosion.

3. Validation

In the underwater explosion, due to a lack of experimental data, the numerical model was validated against analytical results. The analytical results were calculated using peak pressure and time decay formulas from underwater explosions by RH Cole. The formulas are as follows:

$$P(t) = P_m e^{-t/\theta} \tag{9}$$

where θ, t, and P_m denote the exponential time decay constant, time, and shock wave peak pressure, respectively. The peak pressure and time decaying constants are as follows:

$$P_m = k_1 \left(\frac{W^{1/3}}{R} \right)^{\alpha_1} \tag{10}$$

$$\theta = k_2 W^{1/3} \left(\frac{W^{1/3}}{R} \right)^{\alpha_2} \tag{11}$$

where W is the weight of explosives and k_1, k_2, α_1, α_2 are constants.

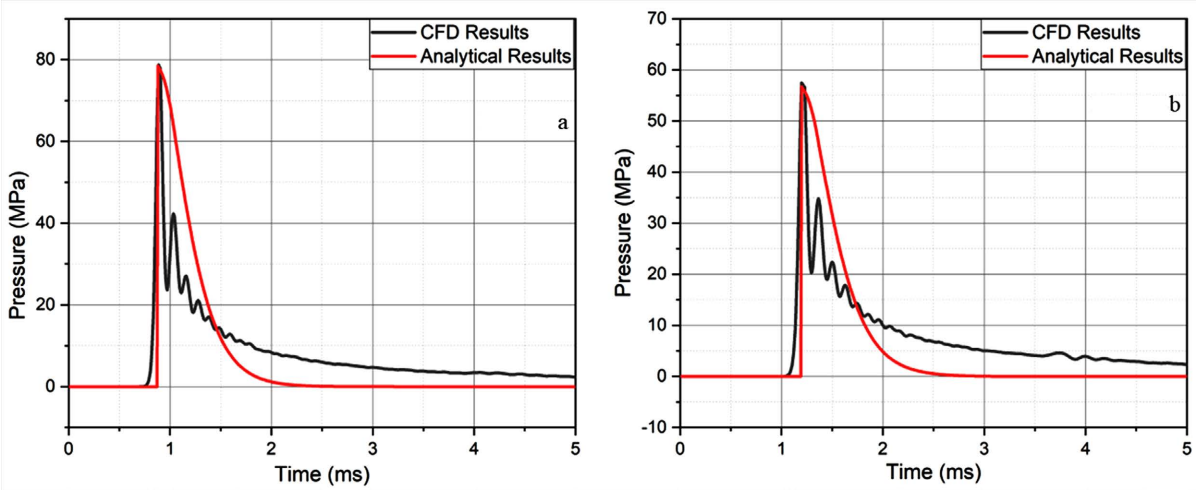

Figure 4. Comparison of present CFD and analytical calculation results at (a) 1.5 m and (b) 2 m from the center of the explosion.

Analytical results for a 10 kg TNT underwater explosion at 1.5 m and 2 m from the center of the explosion were calculated using the above equations and compared to the CFD results. The shock wave propagation was shown in **Figure 2(b)** at time $t = 1$ ms. The comparison of present CFD and analytical results is shown in **Figure 4(a)** and **Figure 4(b)**. It shows the shock front reaches its peak instantly and then returns quasi-exponentially to its initial values. The pressure-time results predicted by the numerical model show good agreement with the analytical results. In **Figure 4(a)** and **Figure 4(b)**, there are a few numerical oscillations following the peak pressure. This may be due to a strong shock wave discontinuity, which cannot be predicted by a numerical model. In this result, the initial shock strength and peak pressure of both the CFD and analytical results match reasonably well. The relative errors of arrival time and peak magnitude are negligible. This shows that this numerical model can predict shock wave propagation and attenuation effects effectively.

4. Results

The explosion near the interface involves complex physical phenomena. Each case follows different flow physics, like reflection, transmission, cavitation, and propagation of a shock wave. In both air and water explosions, the shock wave approaches two types of boundaries. The first one is a free surface, and the other is a fluid-structure interaction. These boundaries have a significant impact on the propagation of shock wave [17]-[20]. Whereas in the interface explosion, the shock wave initially hits the interface and propagates in both air and water. Depending upon the medium of the explosion, the shock wave attenuation varies considerably. The computational domain for all three cases was modeled using an Euler sub-grid, which includes water, and air separated by an interface, and TNT was positioned. The domain is symmetric about the y-axis. The explosion charge is positioned 1 meter below the interface for Case 1, 1 meter above the interface

for Case 2, and in the interface for Case 3. The charge weight is 10 kg. The transmitting boundary is employed in these simulations to avoid the effects of reflected shock wave. The monitoring points were fixed in the vertical direction symmetric to the charge center to calculate the flow field variables.

4.1. Underwater Explosion Near Free Surface (Case 1)

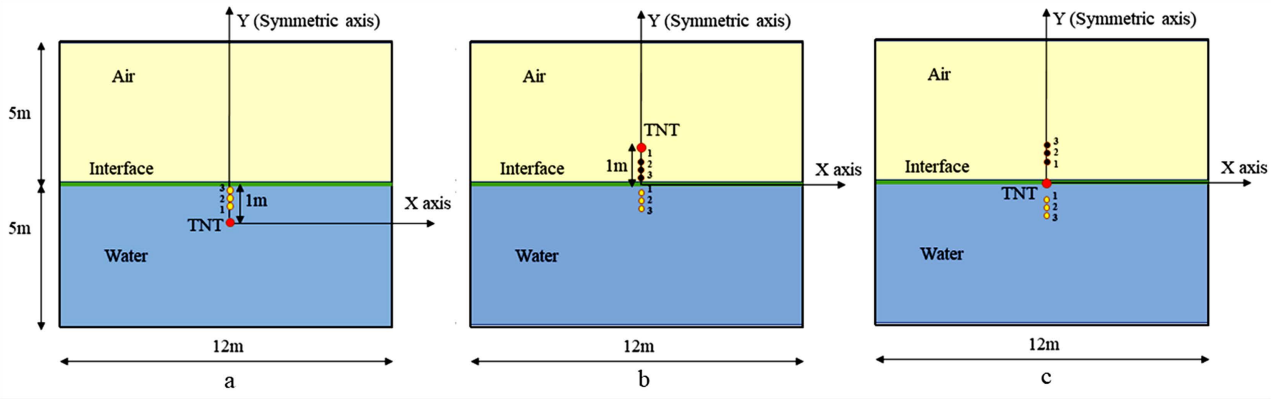

Figure 5. (a) Computational domain of Case 1) Underwater explosion near free surface. Monitoring points are fixed at 0.2 m, 0.4 m, and 0.6 m below the water-air interface. (b) Computational domain of Case 2) Explosion above the free surface. Monitoring points fixed at 0.2 m, 0.4 m, and 0.6 m below and above the air-water interface. (c) Computational domain of Case 3) Explosion at the free surface. Monitoring points are fixed at 0.6 m, 0.8 m, and 1.0 m above and below the interface.

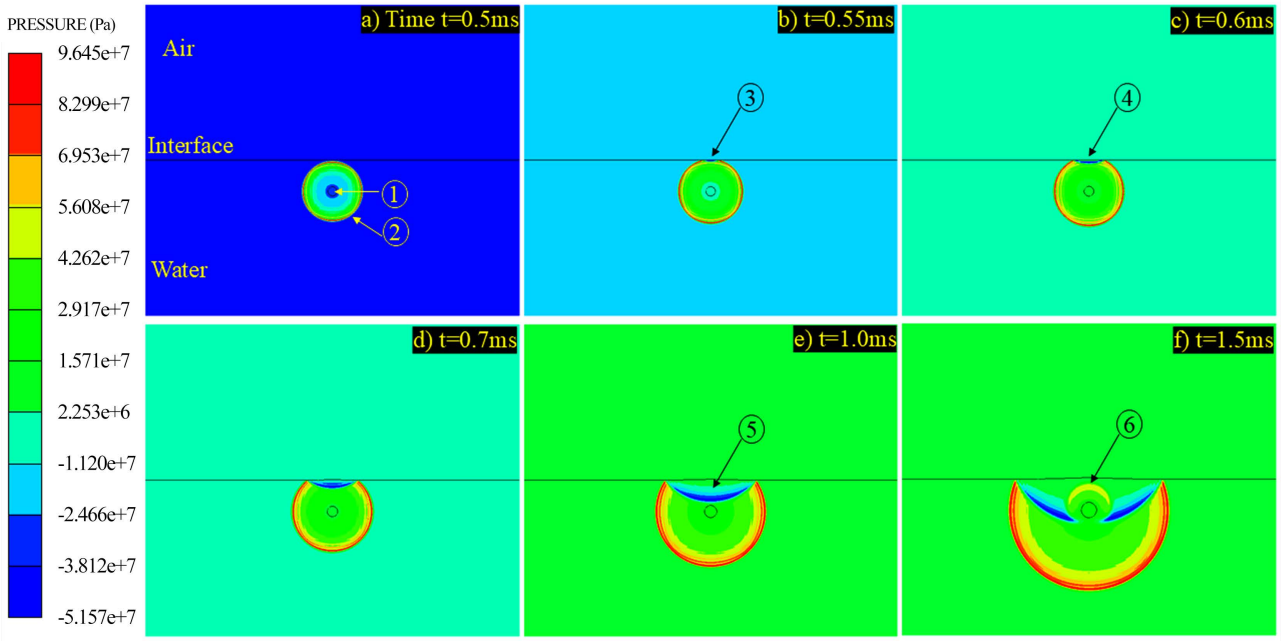

Figure 6. Pressure contour of Case 1) Explosion in water. Key Features 1. Center of Explosion. 2. Shock front. 3. Shock wave reflection at interface. 4. Initiation of cavitation. 5. Cavitation zone. 6. Secondary reflected shock wave due to gas bubble.

Figure 5(a) shows the computational domain of Case 1: explosion in water. After the detonation of the charge, the spherical shock front radiates out from the center as shown in Figure 6(a). The shock wave propagates and moves toward the

free surface, as shown in Figure 6(b). Once the initial shock front interacts with the water-air interface, the shock wave transmits into the air medium, and the compression shock wave reflects as a tensile reflected wave as shown in Figure 6(c). At 1 atm and 15˚C, the acoustic impedance of air and water is 410 and 1.5×10^6 kg·m^{-2}·s^{-1} respectively. These values show that the acoustic impedance of water is nearly 3500 times higher than that of air. Due to the huge difference in acoustic impedance between air and water, the transmitted shock is much weaker compared to the reflected rarefaction waves. Due to this reason, the transmitted shock is not visible in Figure 6(d). The reflected shock wave has the same strength as the incident shock wave. Since water cannot withstand significant tension, the reflected rarefaction wave causes a sudden decrease in water pressure that results in cavitation, as shown in Figure 6(e). As the propagation of the rarefaction wave continues, the pressures of the incident and reflected waves cancel each other, resulting in a very large cavitation zone beneath the free surface, as shown in Figure 6(e). Further, the reflected waves interact with the gas bubble at the center of the explosion, which results in a secondary reflected shock wave as shown in Figure 6(f).

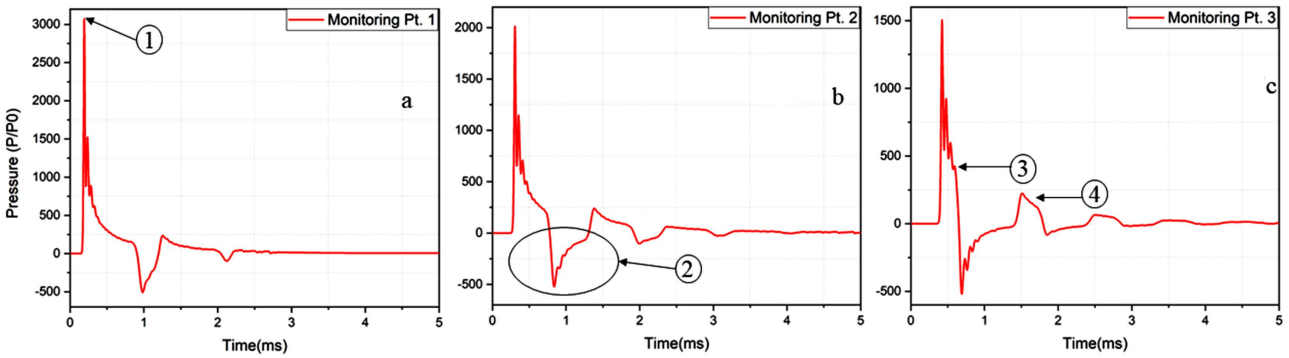

Figure 7. Pressure-Time history graph at different monitoring points. (a) 0.6 m (b) 0.4 m and (c) 0.2 m below the interface. Key Features 1. Peak pressure of incident shock wave. 2. Cavitation zone due to negative pressure. 3. Arrival of reflected shock wave. 4. Secondary reflected shock wave.

The pressure time histories of monitoring points near the interface are depicted in Figure 7. The monitoring points are fixed at 0.2 m, 0.4 m, and 0.6 m below the water-air interface, respectively. The results show that the incident shock front has a pressure ratio of nearly 3000 at monitoring point 1 and attenuates at points 2 and 3, respectively as shown in Figure 7. At monitoring point 3, which is very close to the interface the incident shock strikes the interface and reflects as shown in Figure 7(c). Because of the very large acoustic impedance difference between air and water, the pressure ratio of the reflected shock reduces abruptly to around −500. The other monitoring points also record similar variations in pressure. This large negative pressure results in a huge cavitation zone near the water-air interface for a few milliseconds. Further, the reflected wave interacts with the initial bubble, resulting in a secondary reflected shock wave, and cavitation due to these secondary reflections is not significant as shown in Figure 7(c).

4.2. Explosion above the Free Surface (Case 2)

Figure 5(b) depicts the computational domain of Case 2: explosion in air. In this case, the explosion medium is air. Once the explosion ignites, the shock wave propagates in all directions as shown in Figure 8(a). The density of air is 1.225 kg/m^3, and the speed of sound propagation is approximately 340 m/s. So, the propagation of shock wave is slower in the air compared to that of water. Figure 8(b) depicts the shock wave approaching and interacting with the air-water interface. Due to the nature of water, the surface of the water almost acts like a solid wall. At time $t = 0.6$ ms, the shock wave impinges on the interface and attempts to transmit inside water and reflect in air, as shown in Figure 8(c). Unlike an explosion in water, both the reflected and transmitted shock waves are compression waves in this case, so both can be seen in Figure 8(e). The density of water is 998 kg/m^3, and the speed of sound in water is nearly 1500 m/s. So once the shock interacts with the interface, it tries to reflect as a compression/shock wave. Also, it propagates inside the water as a compression/shock wave as shown in Figure 8(f).

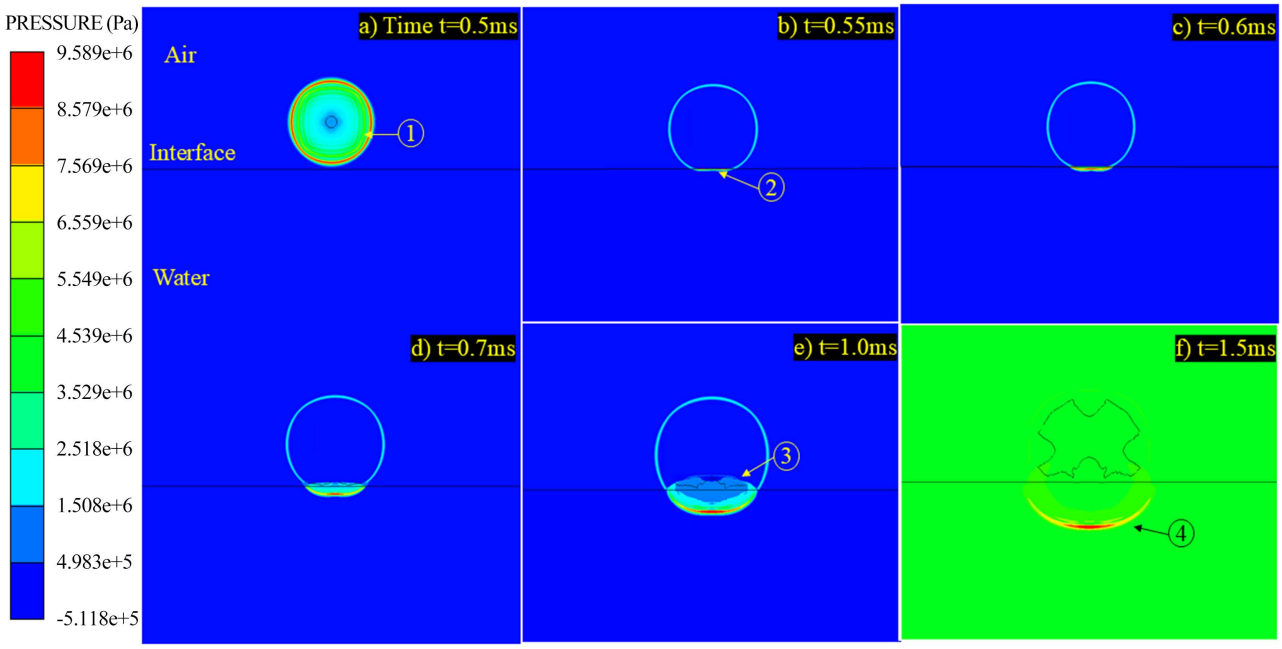

Figure 8. Pressure contour of Case 2) Explosion in air. Key Features 1. Shock front. 2. Shock wave interaction at interface. 3. Reflected shock wave 4. Transmitted shock wave.

Figure 9 shows the pressure time histories of Case 2 Explosion in air. The monitoring points were fixed above and below the interface at a distance of 0.2 m, 0.4 m, and 0.6 m, respectively, as shown in Figure 5(b). As the incident shock approaches the interface, the pressure ratio at monitoring point 1 is around 40 and attenuates further at the 2nd and 3rd monitoring points to 27.6 and 20.4, respectively as shown in Figure 9(b) and Figure 9(c). Once the shock impinges on the air-water interface, the water almost acts like a solid body, so the reflected shock

strength measured at monitoring point 3 is higher than that of the incident shock as shown in Figure 9(c). The reflected shock attenuates gradually, and other monitoring points record lower values as shown in Figure 9. In this case, the arrival of secondary shock wave reflection due to the presence of an air-water interface is shown in Figure 9(c) and it dissipates immediately due to its weak shock strength.

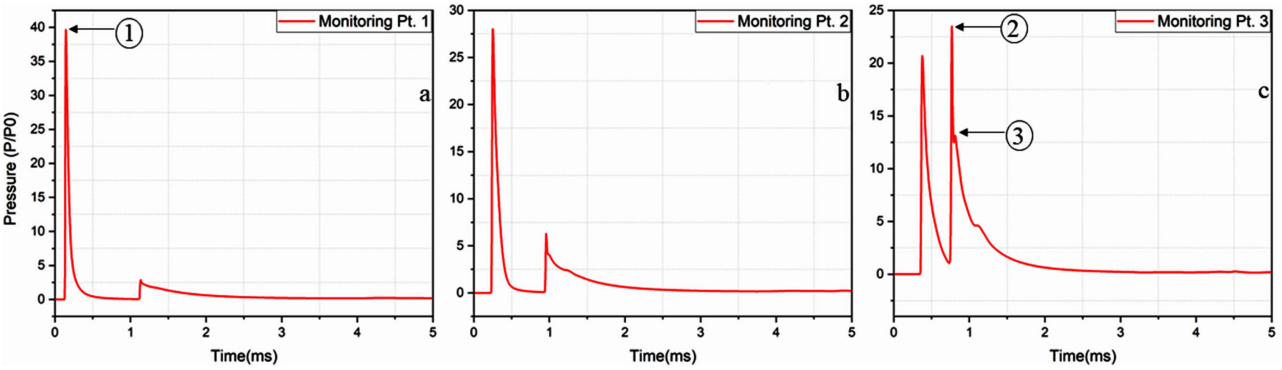

Figure 9. Pressure-Time history graph at different monitoring points. (a) 0.6 m (b) 0.4 m and (c) 0.2 m above the interface. Key Features 1. Peak pressure of incident shock wave. 2. Reflected shock wave. 3. Secondary shock wave reflection.

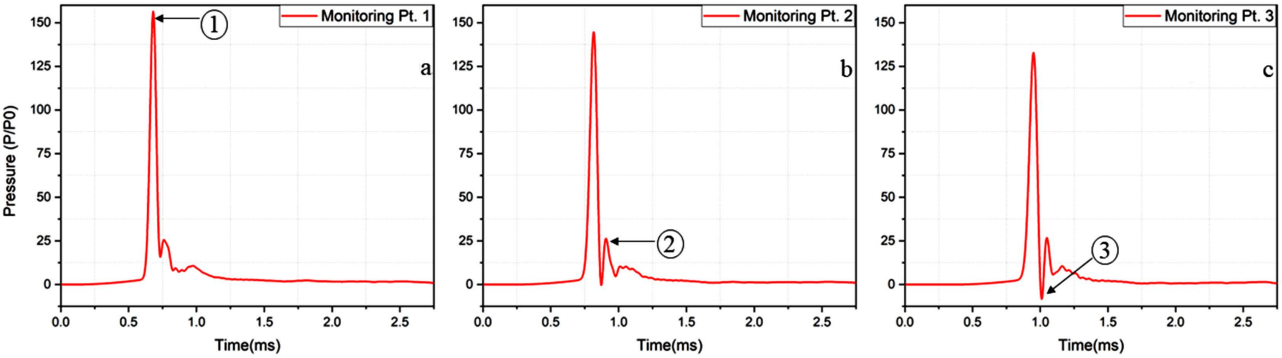

Figure 10. Pressure-Time history graph at different monitoring points. (a) 0.2 m (b) 0.4 m and (c) 0.6 m below the interface. Key Features 1. Peak pressure of incident shock wave. 2. Secondary shock wave. 3. Cavitation due to negative pressure.

The monitoring points in Figure 10 recorded the pressure time histories of the transmitted shock wave in the water region. Once the incident shock interacts with the air-water interface, the monitoring points near the interface experience a considerable transmitted shock wave, as shown in Figure 10. At monitoring point 1, the shock wave pressure ratio is around 153, and it attenuates gradually in monitoring points 2 and 3 as shown in Figure 10. The shock wave propagates as a compression wave in the water medium, but once it crosses, it experiences a smaller negative pressure variation and the secondary shock waves as shown in Figure 10(c). As per Classical Nucleation Theory (CNT), water has a strong, cohesive nature and can withstand a tensile stress or negative pressure of nearly 100 MPa [18]. as the negative pressure recorded at these monitoring points is very minimal and not able to withstand considerable time. Hence, the cavitation in these regions is neglected. In this case, both reflected shock and transmitted shock

wave are significant. The magnitude of the transmitted shock wave is higher in water due to its acoustic impedance.

4.3. Explosion at Air-Water Interface (Case 3)

Figure 5(c) shows the computational domain of Case 3: Explosion at the interface. In this case, the explosive charge is fixed exactly at the interface. Once the explosion occurs, the shock wave approaches both air and water equally as shown in Figure 11(a). As the explosion happens at the interface, it deforms the air-water interface and the acoustic impedance of water is very high; the shock wave that tries to enter water experiences a considerable reflection at the interface as shown in Figure 11(b). At time $t = 0.3$ ms, the reflected shock from water joins the incident shock that is propagating in the air medium as shown in Figure 11(c). Hence, initially, the incident shock wave propagation in both air and water is significant as shown in Figure 11(d). Then the shock wave attenuates at a faster pace in air compared to water due to the nature of the respective medium as shown in Figure 11(e). The shock front pressures for air and water are of different magnitudes due to their huge acoustic impedance differences. At time $t = 1$ ms, the magnitude of the shock front in the air side is weak compared to that of water as shown in Figure 11(f).

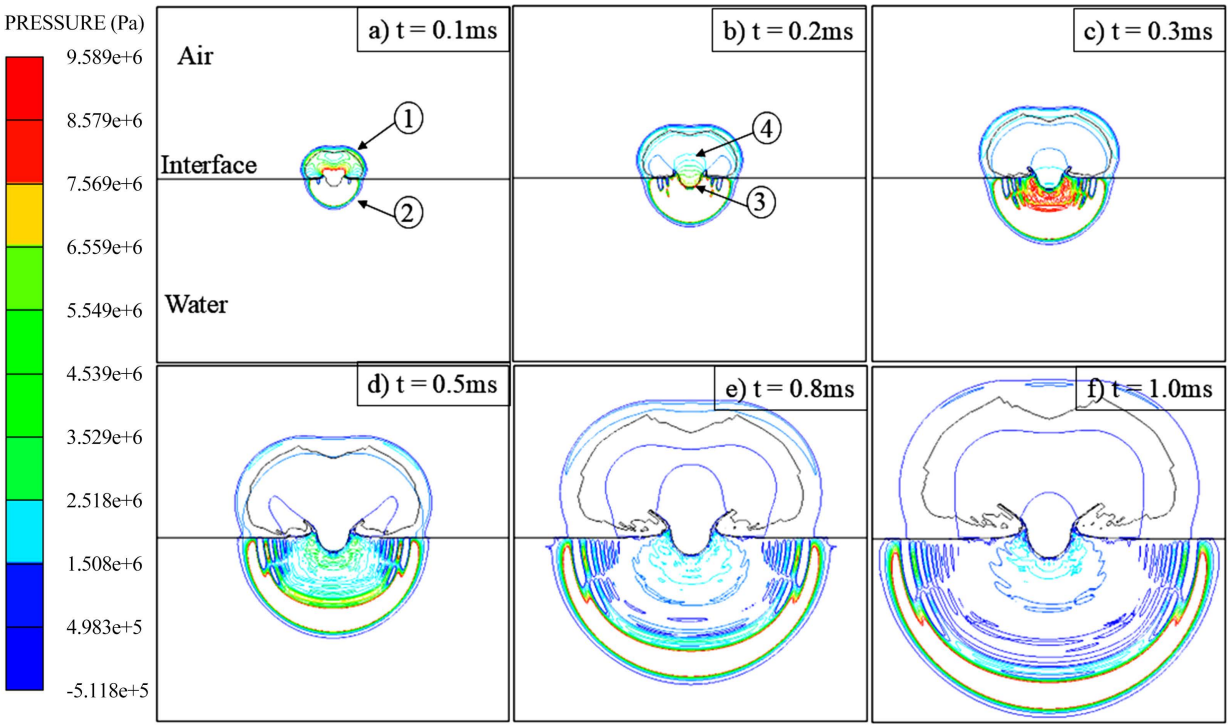

Figure 11. Pressure contour of Case 2) Explosion at the interface. Key Features 1. Incident shock front in air. 2. Shock front in water 3. Deformation of interface. 4. Reflected shock wave due to interface.

Figure 12 shows the pressure time histories of monitoring points fixed near the interface. In this case, the monitoring point was fixed at 0.6 m, 0.8 m, and 1 m

below and above the interface, respectively. Monitoring points were fixed a little far because the initial explosion has a very high magnitude compared to other gauge points. To avoid those initial effects, the monitoring points were fixed slightly away from the interface in this case. The shock wave propagates as a compression wave in the air medium, as shown in Figure 12(a). It reaches a peak and drastically attenuates at all monitoring points, as shown in Figure 12(a). In water, the shock wave also enters as a compression wave, as shown in Figure 12(b). Once the shock crosses the monitoring point, it experiences secondary shock and it gradually attenuates. In this case, the monitoring points record small negative wiggles in Figure 12(b) but the strength of those negative pressure profiles is negligible.

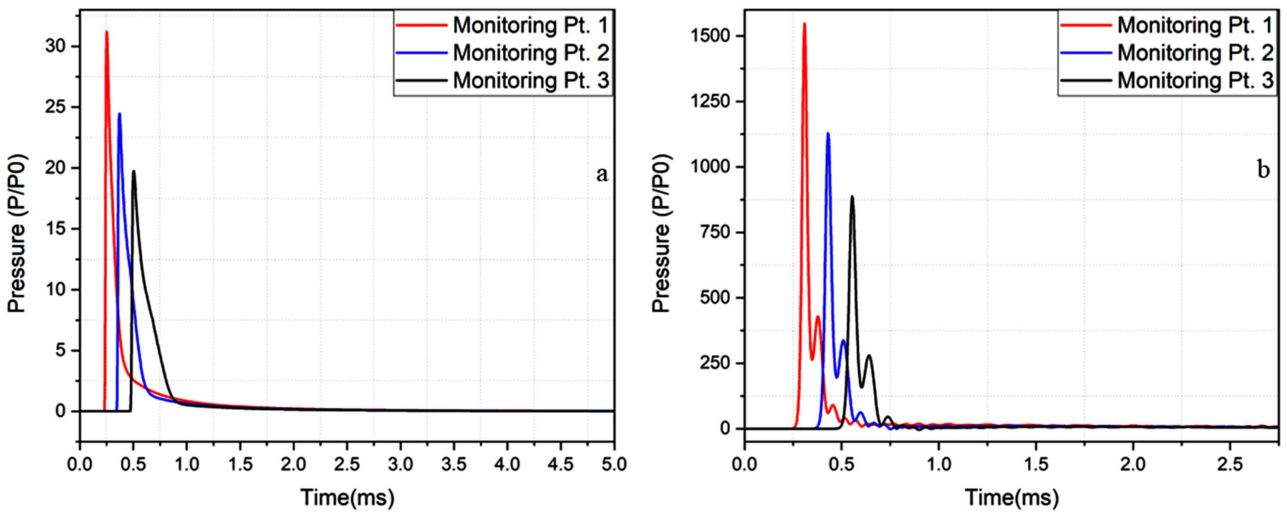

Figure 12. Pressure-Time history graph at 0.6 m, 0.8 m, and 1.0 m (a) above (in air) and (b) below (in water) the interface.

5. Discussion

5.1. Shockwave Propagation Near Free Surface

Figure 13 shows the wave diagram of all three cases. In this analysis, the characteristics of shockwave propagation are discussed in detail. This graph shows that the region from 0 - 5 m in the x-axis is filled with water, 5 - 10 m is filled with air, and the water-air interface (free surface) was fixed at 5 m in all three cases. Whereas the explosion is fixed at 4 m (1 m below the interface) for Case 1, at 6 m (1 m above the interface) for Case 2, and at 5 m (at the air-water interface) for Case 3. Figure 13(a) depicts the wave diagram of an underwater explosion. In this case, TNT is fixed at 1 m below the interface in the water medium and explodes at time $t = 0$. The shock propagates in water and it approaches the water-air interface at time $t = 0.5$ ms. The shock wave reflects and transmits due to the effect of the interface. The difference in acoustic impedance between air and water is very high. Because of that the reflected expansion wave drops below the ambient pressure and results in cavitation and the transmitted shock is very minimal, as shown in Figure 13(a). The strength of the reflected and incident shock wave is of equal

magnitude; the reflected rarefaction wave propagates in water as does the incident shock wave, as shown in Figure 13(a).

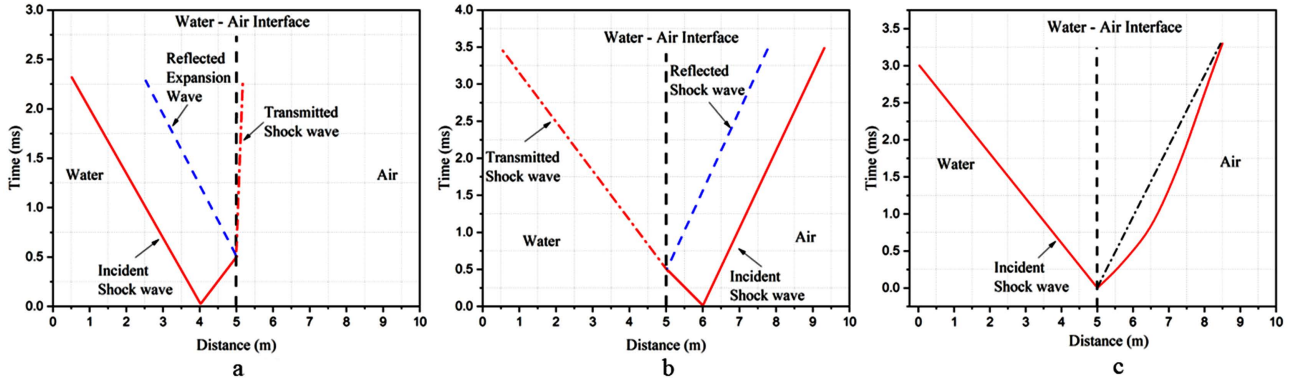

Figure 13. X-T wave diagram of (a) Explosion in water; (b) Explosion in air; (c) Explosion at the interface.

In Case 2, the explosion is fixed at 1 m above the interface in the air medium, as shown in Figure 13(b). The remaining conditions are identical to those in Case 1. After the explosion, the shock wave moves toward the air-water interface (free surface). When the shock wave reaches the interface, part of it transmits into the water and the other part reflects in the air region, as shown in Figure 13(b). Due to the cohesive nature of water, the reflected shock wave and transmitted shock wave are strong compression waves. The speed of sound in water is around 1500 m/s, so the transmitted shock wave propagates inside the water medium faster compared to that of the reflected wave in the air medium, as shown in Figure 13(b). In Case 3, the explosion is fixed at the interface. After the explosion, the shock wave propagates in both regions as shown in Figure 13(c). Initially, the shock wave propagated in the air at a faster pace. This could be caused by the reflected wave from the interface interacting with the incident wave in the air medium. But as time proceeds, the attenuation of shock wave in the air is higher than that of water. So, the shock gets weaker in magnitude and is not able to propagate a greater distance. Hence a significant bend in the curve was able to be noticed in the air region and it was compared against the imaginary line as shown in Figure 13(c). The imaginary line is a shock wave propagation pattern without the effect of the interface. On the other hand, the shock wave in water experiences a significantly higher magnitude of shock wave due to its acoustic impedance. Furthermore, water has a much higher density and sound speed than air, allowing it to transmit shock wave at a much faster rate.

5.2. Effect of Acoustic Impedance in Shockwave Attenuation

Figure 14 shows the comparison of shock wave attenuation in air, water, and interface explosions. The Euler number is used as the scaling parameter to compare the results of air and water. Density and speed of sound are the major parameters that differentiate air from water. To compare the results of air, water, and interface explosions, the Euler number is plotted against the distance to study the attenua-

tion effect of the shock wave in different mediums of explosion. In all cases, once an explosion initiates from the center, the shock wave reaches its peak at each monitoring point and attenuates with respect to time. In this graph, the monitoring points were fixed at 1 m, 2 m, 3 m, and 4 m from the charge to measure the flow field variables, and the Euler number was calculated at each point. For water and air explosion, all four monitoring points are fixed at the water and air medium, respectively. In an interface explosion, four monitoring points each are fixed on both the air and water medium from the charge center.

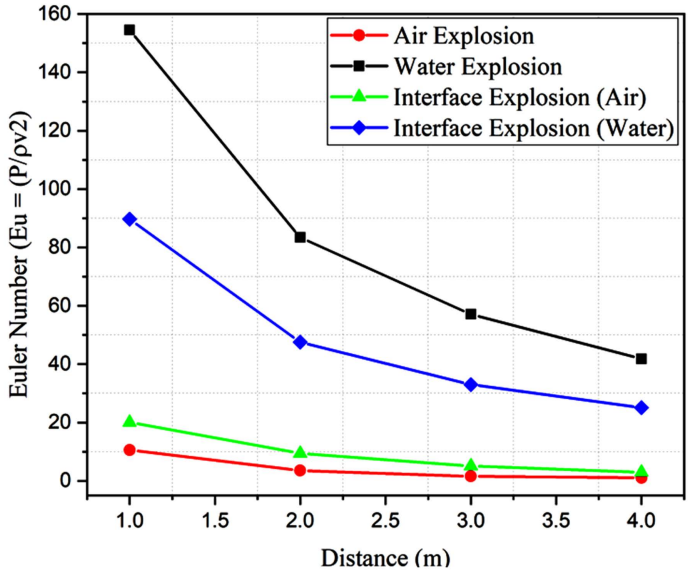

Figure 14. Comparison of shock wave attenuation of explosion in air, water, and interface.

In water explosion, the Euler number at the initial point is 154.49 followed by 83.4, 57.08, and 41.81 respectively. Meanwhile, in the case of air explosions, the Euler numbers were 10.59, 3.53, 1.56, and 1.05, respectively. The Euler number calculated at each location for water explosion (Case 1) is significantly higher than that of air explosion (Case 2). Also, the shock wave in water attenuates gradually, whereas, in the air, it reaches its minimum within a shorter time scale as shown in **Figure 14**. This major difference is due to the cohesive nature of water and the acoustic impedance difference between the respective mediums. Interface explosions have both air and water sides, shock wave attenuation on the waterside (Case 3) is similar to water explosions (Case 1). The calculated Euler numbers are 89.69, 47.53, 32.99, and 25.11 respectively. The magnitude is considerably lower than in Case 1 due to the transmission of shock wave through the interface. However, the magnitude of the explosion on the air side of the interface (Case 3) is 20.07, 9.44, 5.14, and 3.00 respectively. It is slightly greater and gradually diminishes when compared to the air-side explosion (Case 2). This could be because the shock wave reflected from the water-air interface during an explosion joins the incident shock wave, resulting in a larger magnitude and slower attenuation than in an air explosion. Hence the graph shows the medium of the explosion near the interface has

a significant impact on the shockwave propagation and attenuation characteristics.

6. Conclusions

This study aims to numerically investigate the shock wave propagation, attenuation, and free surface effects for different mediums of explosion. In an underwater explosion, the shock wave reaches the interface and is reflected in the water as an expansion wave and transmitted in the air as a weak shock wave due to the acoustic impedance of water. Cavitation happened near the free surface when the reflected expansion wave abruptly dropped to extremely negative pressure. In an air explosion, the shock wave reaches the free surface and reflects as a compression wave. Due to the cohesive nature of water, the free surface acts like a solid body, and the reflected shock wave is of equal magnitude to that of the incident shock wave. Unlike underwater explosions, the transmitted shock, in this case, propagates as a strong compression shock wave.

In an explosion at the air-water interface, the shock wave propagates at different magnitudes in air and water. In both air and water regions, it reaches the peak pressure and then reduces exponentially back to the ambient pressure. The water region experiences minor negative pressure fluctuations, which are insufficient to cause cavitation. The comparison of results shows that the shock wave in an air medium attenuates faster than in a water medium. Because the density and speed of sound in water are much higher than those in air, shock wave propagation and mitigation behavior differ significantly. In contrast, due to the effect of the free surface, slightly higher pressure magnitudes are experienced on the air side of the interface explosion compared to that of the explosion in the air. This may be due to a reflection of the shock wave at the free surface, which joins with the incident shock in the air medium. So, the shock wave propagates faster initially in the air medium and gradually attenuates. Whereas, due to the effect of the free surface, the shock that enters the water medium has a slightly lower magnitude compared to that of an explosion in the water. Hence, in this study, the characteristics of shock wave propagation and attenuation in air, water, and interface were studied, and the results were compared. This study shows the free surface near different mediums of the explosion has a considerable effect on shock wave propagation, attenuation characteristics, and flow physics in explosion-related studies.

Acknowledgements

This work was supported by a Research Grant from Andong National University.

Conflicts of Interest

The authors declare no conflicts of interest regarding the publication of this paper.

References

[1] Needham, C.E. (2010) Blast Waves. Springer.

[2] Liu, T.G., Khoo, B.C., Yeo, K.S. and Wang, C. (2003) Underwater Shock-Free Surface-Structure Interaction. *International Journal for Numerical Methods in Engineering*, **58**, 609-630. https://doi.org/10.1002/nme.791

[3] Molyneaux, T.C.K., Li, L. and Firth, N. (1994) Numerical Simulation of Underwater Explosions. *Computers & Fluids*, **23**, 903-911. https://doi.org/10.1016/0045-7930(94)90060-4

[4] Wu, W., Liu, Y., Zhang, A., Liu, N. and Liu, L. (2020) Numerical Investigation on Underwater Explosion Cavitation Characteristics Near Water Wave. *Ocean Engineering*, **205**, Article 107321. https://doi.org/10.1016/j.oceaneng.2020.107321

[5] Xiao, W., Wei, H. and Feng, L. (2017) Investigation on the Cavitation Effect of Underwater Shock Near Different Boundaries. *China Ocean Engineering*, **31**, 396-407. https://doi.org/10.1007/s13344-017-0046-x

[6] Daramizadeh, A. and Ansari, M.R. (2015) Numerical Simulation of Underwater Explosion Near Air-Water Free Surface Using a Five-Equation Reduced Model. *Ocean Engineering*, **110**, 25-35. https://doi.org/10.1016/j.oceaneng.2015.10.003

[7] Cui, P., Zhang, A.M. and Wang, S.P. (2016) Small-Charge Underwater Explosion Bubble Experiments under Various Boundary Conditions. *Physics of Fluids*, **28**, Article 117103. https://doi.org/10.1063/1.4967700

[8] Nguyen, V., Phan, T., Duy, T. and Park, W. (2021) Numerical Modeling for Compressible Two-Phase Flows and Application to Near-Field Underwater Explosions. *Computers & Fluids*, **215**, Article 104805. https://doi.org/10.1016/j.compfluid.2020.104805

[9] Phan, T., Nguyen, V. and Park, W. (2019) Numerical Study on Dynamics of an Underwater Explosion Bubble Based on Compressible Homogeneous Mixture Model. *Computers & Fluids*, **191**, Article 104262. https://doi.org/10.1016/j.compfluid.2019.104262

[10] Cole, R.H. (1948) Underwater Explosions. Princeton University Press. https://doi.org/10.5962/bhl.title.48411

[11] Kedrinskii, V.K. (1976) Negative Pressure Profile in Cavitation Zone at Underwater Explosion Near Free Surface. *Acta Astronautica*, **3**, 623-632. https://doi.org/10.1016/0094-5765(76)90166-1

[12] Wang, G., Zhang, S., Yu, M., Li, H. and Kong, Y. (2014) Investigation of the Shock Wave Propagation Characteristics and Cavitation Effects of Underwater Explosion Near Boundaries. *Applied Ocean Research*, **46**, 40-53. https://doi.org/10.1016/j.apor.2014.02.003

[13] Rajendran, R. and Lee, J.M. (2009) Blast Loaded Plates. *Marine Structures*, **22**, 99-127. https://doi.org/10.1016/j.marstruc.2008.04.001

[14] Librescu, L., Oh, S. and Hohe, J. (2006) Dynamic Response of Anisotropic Sandwich Flat Panels to Underwater and In-Air Explosions. *International Journal of Solids and Structures*, **43**, 3794-3816. https://doi.org/10.1016/j.ijsolstr.2005.03.052

[15] Rajasekar, J., Kim, T.H. and Kim, H.D. (2020) Visualization of Shock Wave Propagation Due to Underwater Explosion. *Journal of Visualization*, **23**, 825-837. https://doi.org/10.1007/s12650-020-00664-9

[16] Worthington, A.M. and Cole, R.S. (1900) Impact with a Liquid Surface Studied by the Aid of Instantaneous Photography. Paper II. *Philosophical Transactions of the Royal Society A*, **194**, 175-199. https://doi.org/10.1098/rsta.1900.0016

[17] Baer, M.R. (1992) A Numerical Study of Shock Wave Reflections on Low Density Foam. *Shock Waves*, **2**, 121-124. https://doi.org/10.1007/bf01415901

[18] Ben-Dor, G. (1992) Shock Wave Reflection Phenomena. Springer. https://doi.org/10.1007/978-1-4757-4279-4

[19] Henderson, L.F. (1989) On the Refraction of Shock Waves. *Journal of Fluid Mechanics*, **198**, 365-386. https://doi.org/10.1017/s0022112089000170

[20] Sembian, S., Liverts, M., Tillmark, N. and Apazidis, N. (2016) Plane Shock Wave Interaction with a Cylindrical Water Column. *Physics of Fluids*, **28**, Article 056102. https://doi.org/10.1063/1.4948274

[21] Aune, V., Fagerholt, E., Hauge, K.O., Langseth, M. and Børvik, T. (2016) Experimental Study on the Response of Thin Aluminium and Steel Plates Subjected to Airblast Loading. *International Journal of Impact Engineering*, **90**, 106-121. https://doi.org/10.1016/j.ijimpeng.2015.11.017

[22] Rajasekar, J., Yaga, M. and Kim, H.D. (2022) Numerical Prediction on the Mitigation of Shock Wave Using Geometric Barriers. *Journal of Visualization*, **26**, 83-96. https://doi.org/10.1007/s12650-022-00866-3

[23] Bakken, J., Slungaard, T., Engebretsen, T. and Christensen, S.O. (2003) Attenuation of Shock Waves by Granular Filters. *Shock Waves*, **13**, 33-40. https://doi.org/10.1007/s00193-003-0180-7

[24] Ye, M., Ma, H. and Ni, Q. (2017) Research on a Sudden Explosion and Its Environmental Impact. *IOP Conference Series*: *Materials Science and Engineering*, **275**, Article 012022. https://doi.org/10.1088/1757-899x/275/1/012022

[25] Cheng, M., Hung, K.C. and Chong, O.Y. (2005) Numerical Study of Water Mitigation Effects on Blast Wave. *Shock Waves*, **14**, 217-223. https://doi.org/10.1007/s00193-005-0267-4

[26] Liu, T.G., Khoo, B.C. and Yeo, K.S. (1999) The Numerical Simulations of Explosion and Implosion in Air: Use of a Modified Harten's TVD Scheme. *International Journal for Numerical Methods in Fluids*, **31**, 661-680. https://doi.org/10.1002/(sici)1097-0363(19991030)31:4<661::aid-fld866>3.0.co;2-g

[27] Liu, H., Zhou, B., Han, X., Zhang, T., Zhou, B. and Gho, W.M. (2020) Numerical Simulation of Water Entry of an Inclined Cylinder. *Ocean Engineering*, **215**, Article 107908. https://doi.org/10.1016/j.oceaneng.2020.107908

[28] Benusiglio, A., Quéré, D. and Clanet, C. (2014) Explosions at the Water Surface. *Journal of Fluid Mechanics*, **752**, 123-139. https://doi.org/10.1017/jfm.2014.255

[29] Turkyilmazoglu, M. (2016) Air Blast Response of Compaction Foam Having a Deformable Front Face Panel Incorporating Fluid Structure Interactions. *International Journal of Mechanical Sciences*, **105**, 340-347. https://doi.org/10.1016/j.ijmecsci.2015.11.010

[30] Turkyilmazoglu, M. (2022) Maximum Wave Run-Up over Beaches of Convex/Concave Bottom Profiles. *Continental Shelf Research*, **232**, Article 104610. https://doi.org/10.1016/j.csr.2021.104610

[31] Li, T., Wang, S., Li, S. and Zhang, A. (2018) Numerical Investigation of an Underwater Explosion Bubble Based on FVM and VOF. *Applied Ocean Research*, **74**, 49-58. https://doi.org/10.1016/j.apor.2018.02.024

[32] Jaiswal, A. (2011) ANSYS ® Explicit Dynamics and AUTODYN® Applications. ANSYS Inc.